Applied Thermal Engineering 50 (2013) 950–956

Contents lists available at SciVerse ScienceDirect

Applied Thermal Engineering

journal homepage: www.elsevier.com/locate/apthermeng

Experimental and numerical investigations of shell-side thermo-hydraulic performances for shell-and-tube heat exchanger with trefoil-hole baffles

Yonghua You [a], Aiwu Fan [a,*], Xuejiang Lai [b], Suyi Huang [a], Wei Liu [a]

[a] School of Energy and Power Engineering, Huazhong University of Science and Technology, 1037 Luoyu Road, Wuhan 430074, China
[b] School of Engineering, Guangdong Ocean University, Zhanjiang 524088, China

HIGHLIGHTS

- Shell-side performance of a heat exchanger with trefoil-hole baffles was studied.
- The Nusselt number of the shell-side is about 4.5 times that without baffles.
- The overall performance index $Nu/\Delta p$ lies in the range of 16–37 kPa^{-1}.

ARTICLE INFO

Article history:
Received 18 March 2012
Accepted 21 August 2012
Available online 30 August 2012

Keywords:
Shell-and-tube heat exchanger
Trefoil-hole baffle
Shell side performances
Experimental investigation
Numerical study

ABSTRACT

Orifice plates have been developed as the support of tubes for shell-and-tube heat exchangers, however, very few related academic literature are available. In the present work, we experimentally investigate the shell-side thermo-hydraulic performance of a shell-and-tube heat exchanger with trefoil-hole baffles (THB-STHXs) under turbulent flow regime. The test data demonstrate that the heat transfer rate is effectively enhanced on the shell side, meanwhile, the flow resistance increases substantially. Moreover, both the heat transfer performance $(NuPr^{-0.333}(\mu_f/\mu_w)^{-0.14})$ and pressure loss (Δp) rise with the increment of the Reynolds number. Based on the experimental results, correlations of the Nusselt number and pressure loss as a function of the Reynolds number are obtained respectively. To analyze the mechanisms of these thermo-hydraulic characteristics, numerical computation is carried out on the basis of a unit channel, which demonstrates that the trefoil-hole baffle could generate high-speed flush, intensive recirculation flow and high turbulence intensity level. As a result, the heat transfer rate is considerably enhanced and the flow resistance increases substantially as well.

1. Introduction

Shell-and-tube heat exchangers (STHXs) are widely used in chemical engineering, petroleum refining and power generation, etc [1]. Lots of energy could be saved by improving the performances of those devices, which depends on both shell side and tube side. A variety of thermal augmentation techniques have been developed and applied for the tube side, such as various types of high-efficient tubes and tube inserts [2–8].

The performance of shell side is more complicated and depends on the baffle elements to a great extent. The traditional segmental-baffle shell-and-tube heat exchangers (SG-STHXs) have been well developed and widely applied for decades [9–12]. Because the working fluid flows across pipes, the shell-side heat transfer rate is effectively enhanced in SG-STHXs. However, the pressure loss and the 'dead' flow region are considerably large. Moreover, the harmful vibration level is high. In order to solve these problems, numerous experimental [13–15] and numerical investigations [16–18] have been conducted and various types of baffles, tubes and their arrangements have been developed [13–15,18–26].

Shell-and-tube heat exchanger with rod baffles is such an improvement, which was originally proposed by Phillips Petroleum Company [20]. The rods act as the support of tubes for low vibration level. On the other hand, flow disturbance caused by the rods leads to a high heat transfer rate [21,22].

The shell-and-tube heat exchanger with spiral baffles is another example which has good thermo-hydraulic performance and low vibration level [23,24]. However, it is difficult to manufacture continuous spiral baffles. For this reason, some researchers used circular plain baffles with two quadrants hollow in the shell side alternately, which can also induce the fluid to flow spirally [25].

* Corresponding author. Tel.: +86 27 87542618; fax: +86 27 87540724.
E-mail addresses: faw@mail.hust.edu.cn, catia315@163.com (A. Fan).

1359-4311/$ – see front matter © 2012 Elsevier Ltd. All rights reserved.
http://dx.doi.org/10.1016/j.applthermaleng.2012.08.034

Nomenclature

A	flow area, m^2
C_p	specific heat of constant pressure, J/(kg K)
d	tube diameter, m
D	characteristic dimension, m
E	mean rate-of-strain tensor, 1/s
f	function
G_k	turbulent kinetic energy generation rate, kg/(m s^3)
h	convective heat transfer coefficient, W/(m^2 K)
k	turbulent kinetic energy, m^2/s^2
K	overall heat transfer coefficient, W/(m^2 K)
L	tube length, m
n	tube number
Nu	Nusselt number
p	static pressure, Pa
Δp	static pressure loss, Pa
q	volumetric flow rate, m^3/s
Q	heat flux, W
Pr	Prandtl number
R	thermal resistance, m^2 K/W
Re	Reynolds number
s	tube distance, m
S	heat transfer area, m^2
T	static temperature, K
ΔT	temperature difference, K
u	velocity, m/s
U	uncertainty; wetted perimeter, m
x	coordinate axis, m
ρ	density, kg/m^3
μ	dynamic viscosity, N s/m^2
δ	gap, m
ε	turbulent kinetic energy dissipation rate, m^2/s^3
λ	thermal conductivity, W/(m K)
σ	turbulent Prandtl number

Subscripts

eff	effective
ex	outlet
f	fluid
i	inner wall of tube; tensor
in	inlet
j	tensor
l	laminar
m	average
o	outer wall of tube
s	shell side
t	tube side; turbulent
w	wall

To reduce the 'dead' flow region and fouling, various orifice plates were developed as the tube support of STHXs, and were applied in heat exchangers for steam generators of nuclear power plants and other fields [26], in which the fluid flows longitudinally through the gaps between the orifice edges and tube walls. The trefoil-hole plates or quatrefoil-hole plates are such examples. They are of good thermo-hydraulic performances and less liable to foul. However, few open reports and publications could be found. Thus, we will experimentally investigate the thermo-hydraulic performances of a shell-and-tube heat exchanger with trefoil-hole baffles (THB-STHX) in the present study. Moreover, a numerical study is conducted to help analyzing the mechanisms of thermal augmentation on the shell side.

2. Experimental investigation

2.1. Geometric configuration

Fig. 1(a) depicts the sketch of a trefoil-hole baffle, on which trefoil holes are broached for the support of tubes, and the fluid flows through the gaps between the tubes and baffles longitudinally. Fig. 2 shows the experimental sample of THB-STHX. The warm fresh water acts as the working fluid of shell side, while cool fresh water flows in the tube side in opposite direction. The shell has a diameter of 100 mm and a length of 2000 mm. Fourteen tubes with a diameter of 14 mm are installed inside the shell with a triangle arrangement. The amount of trefoil-hole baffle is five with a pitch of 350 mm. The thickness of the baffle is 3 mm, and the size of breach (δ) is 2 mm (see Fig. 1(b)). The detailed structural parameters are listed in Table 1.

2.2. Experimental device and approach

The experimental system is schematically shown in Fig. 3. Besides the test sample of THB-STHX, the experimental setup consists of two loops, i.e., the warm water loop and cool water loop. The warm water is recycled with a centrifugal pump and a reservoir, and a heat pump water heater (HPWH) is adopted to keep the inlet water temperature constant. The cool water loop is an open one, i.e., the cool water is discharged after it is warmed up by warm water in the heat exchanger. In order to minimize the heat loss to the environment, the shell is thermally insulated during the experiment.

Four platinum resistance thermometers (Pt100) with a precision of 0.15 K are used to measure the fluid temperatures at the inlets and outlets of shell and tube sides, as shown in Fig. 3. Two differential pressure transducers are adopted to measure the pressure drops of shell and tube sides, respectively. Two turbine flow meters with an accuracy of 0.5% are arranged in the downstream of tubes to measure the volumetric flow rate of shell and tube sides. In addition, several valves of manual control are used to adjust the temperature and flow rate of the working fluids. All the analog signals of the temperature, pressure difference and flow rate are transmitted to the computer via a Data Acquisition Card (PC-7488), and processed through a software.

2.3. Data reduction

In the present study, the thermo-hydraulic performances of the shell side are characterized by the Nusselt number, Nu and pressure loss, Δp. The latter could be directly measured by a differential pressure transducer, while the acquisition of the former is a little more complicated. The detailed procedure is described as below.

As mentioned above, the shell is thermally insulated and the system is in a steady state during the experiment. Thus, the amount of heat transferred from the shell side to tube side equals to the enthalpy increment of cool water, or the enthalpy decrement of warm water, as shown in Eq. (1).

$$Q = \rho_t q_t C_{p,t} \Delta T_t = -\rho_s q_s C_{p,s} \Delta T_s \tag{1}$$

The overall heat transfer coefficient K could be calculated through Eq. (2).

$$K = \frac{Q}{S \cdot \Delta T_m} \tag{2}$$

where S stands for the heat transfer area based on the outer diameter of tubes, and ΔT_m is the logarithm averaged temperature

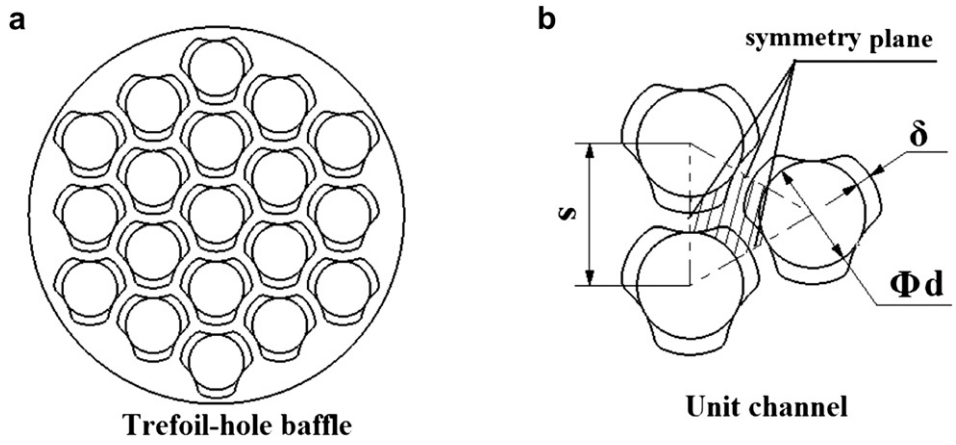

Fig. 1. Trefoil-hole baffle with a triangle arrangement (a), and corresponding unit channel (b).

difference between the warm and cool water, which is calculated through Eq. (3).

$$\Delta T_{\mathrm{m}} = \frac{\Delta T_{\mathrm{in}} - \Delta T_{\mathrm{ex}}}{\mathrm{Ln}\dfrac{\Delta T_{\mathrm{in}}}{\Delta T_{\mathrm{ex}}}} \tag{3}$$

where ΔT_{in} and ΔT_{ex} refer to the fluid temperature differences between the shell side and tube side at the inlet and outlet, respectively.

Since the heat exchanger is newly manufactured, the fouling on the tube surfaces could be neglected. Thus, the convective heat transfer coefficient of the shell side, h_{s}, could be calculated through Eq. (4).

$$h_{\mathrm{s}} = \frac{1}{\dfrac{1}{K} - \dfrac{1}{h_{\mathrm{t}}}\cdot\dfrac{d_{\mathrm{o}}}{d_{\mathrm{i}}} - R_{\mathrm{w}}} \tag{4}$$

where h_{t} is the convective heat transfer coefficient of the tube side, and R_{w} refers to the thermal resistance of tube wall, as shown in Eq. (5).

$$R_{\mathrm{w}} = \frac{d_{\mathrm{o}}}{2\lambda_{\mathrm{w}}}\cdot\mathrm{Ln}\frac{d_{\mathrm{o}}}{d_{\mathrm{i}}} \tag{5}$$

where λ_{w} is the conductivity of tube wall.

The flow on the tube side is also turbulent, and its convective heat transfer coefficient h_{t} is calculated through Eq. (6) [27].

$$\frac{h_{\mathrm{t}}D_{\mathrm{t}}}{\lambda_{\mathrm{t,f}}} = 0.027Re_{\mathrm{t}}^{0.8}Pr_{\mathrm{t}}^{1/3}\left(\frac{\mu_{\mathrm{t,f}}}{\mu_{\mathrm{t,w}}}\right)^{0.14} \tag{6}$$

where D_{t} is the characteristic dimension of the tube side (equals to the inner diameter of tubes), while Re_{t} is the Reynolds number of tube side, which could be calculated through Eq. (7).

$$Re = \frac{\rho u D}{\mu} \tag{7}$$

The Reynolds number on the shell side is also determined by Eq. (7), where the average velocity far from the baffle acts as the characteristic velocity, while the characteristic dimension D is calculated through Eq. (8).

$$D = \frac{4A}{U} \tag{8}$$

Finally, the Nusselt number on the shell side could be obtained with Eq. (9).

$$Nu = \frac{hD}{\lambda} \tag{9}$$

2.4. Results and discussions

The mass flow rate on the shell side varies from 6.9 to 13.9 kg/s in the experiment, corresponding to the shell-side Reynolds

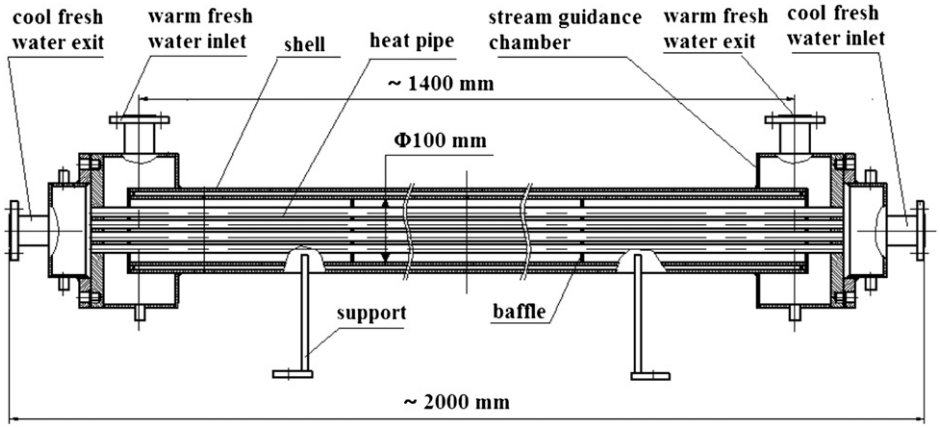

Fig. 2. Assembly drawing of the test sample of THB-STHX.

Table 1
Structural parameters of the THB-STHX.

Material: Stainless steel	
Tube inner diameter: 12 mm	Tube outer diameter: 14 mm
Tube arrangement: Triangle	Tube distance (s): 19 mm
Tube number: 14	Tube effective length: 1400 mm
Shell inner diameter: 100 mm	
Baffle number: 5	Baffle pitch: 350 mm
Baffle thickness: 3 mm	Breach number: 3
Breach size (δ): 2 mm	

number from ~10,000 to 25,000. Fig. 4 shows the variation of the dimensionless parameter $NuPr^{-0.333}(\mu_f/\mu_w)^{-0.14}$ with the Reynolds number, and the counterpart of the case without baffles (calculated through Eq. (6)) is depicted in the same figure with a dot–dot–dash line for comparison. It is noted that the average dimensionless parameter of the THB-STHX is ~280, which is about 4.5 times that of the cases without baffles. This demonstrates that the THB-STHX has a good performance of heat transfer. Moreover, the heat transfer rate increases with the increment of the Reynolds number. The dimensionless parameter is fitted by an empirical formula, as shown in Eq. (10), and also plotted in Fig. 4 (solid line).

$$Nu = 0.0328Re^{0.9337}Pr^{0.333}\left(\frac{\mu_f}{\mu_w}\right)^{0.14}, \quad 10,000 < Re < 25,000 \tag{10}$$

The behavior of flow resistance is presented in Fig. 5, and the counterpart of the case without baffles is calculated through Blasius correlation (see Eq. (11)) [27], and plotted in the same figure with a dotted line for comparison.

$$\Delta p = \frac{0.3164}{Re^{0.25}}\cdot\frac{L}{D}\cdot\frac{\rho u^2}{2} \tag{11}$$

From Fig. 5 it is clearly seen that the shell-side pressure loss of the THB-STHX is much higher than that of the case without baffles (dotted line). Moreover, the pressure loss rises with the increment of the Reynolds number, and the larger the Reynolds number, the larger the increasing rate is. The shell-side flow resistances of the THB-STHX are fitted by an empirical formula, as shown in Eq. (12), and plotted in Fig. 5 as well (solid line).

$$\Delta p = 0.0063032Re^{1.5512}, \quad 10,000 < Re < 25,000 \tag{12}$$

The combined parameter, $Nu/\Delta p$, is fitted by using a three-order polynomial function. Both the measured data and fitted curve are presented in Fig. 6 to illustrate the variation tendency of $Nu/\Delta p$ with the Reynolds number. It is noted that the value of $Nu/\Delta p$ ranges from 16 kPa^{-1} to 37 kPa^{-1} over the Re range under investigation. Moreover, it is also seen in Fig. 6 that the fitted curve has a critical Re number of 18,000. When the Reynolds number is lower than 18,000, the value of $Nu/\Delta p$ drops with the increment of the Reynolds number at a decreasing rate. Inversely, when Reynolds exceeds the critical point, the combined parameter keeps approximately constant.

In addition to the combined parameter, $Nu/\Delta p$, some researchers also used the dimensionless rate of entropy generation to evaluate the overall thermal–hydraulic performance. Nevertheless, the latter is always applied for the optimization of heat transfer processes or heat exchangers [28]. Thus, we do not present its variation tendency here.

The uncertainties of the experimental quantities are determined with the method of Ref. [29], which involves calculating derivatives of variables with respect to individual experimental quantities and applying already known uncertainties, as shown in Eq. (13).

$$U_R = \sqrt{\sum_{i=1}^{n}\left(\frac{\partial R}{\partial x_i}U_{xi}\right)^2} \tag{13}$$

where $R = f(x_1, x_2, \ldots, x_n)$ represents a desired variable, $x_1, x_2, \ldots, x_n$ are the variables that impact R, and their absolute uncertainties are expressed by $U_{x1}, U_{x2}, \ldots, U_{xn}$, respectively.

According to the measurement precisions of platinum resistance thermometers and turbine flow meters, etc., the uncertainties of Q and Nu could be deduced from Eqs. (1) and (9), which are around ±4% and ±15%, respectively. For the convenience to check the

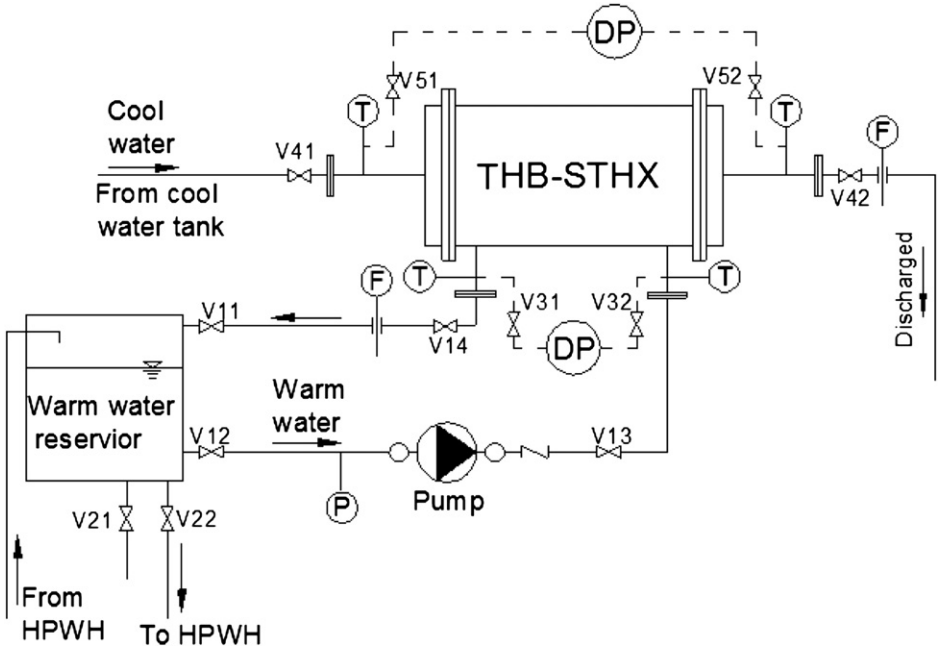

Fig. 3. Schematic of the experimental system. T is platinum resistance thermometer; DP is differential pressure transducer; F is flowmeter; V is valve.

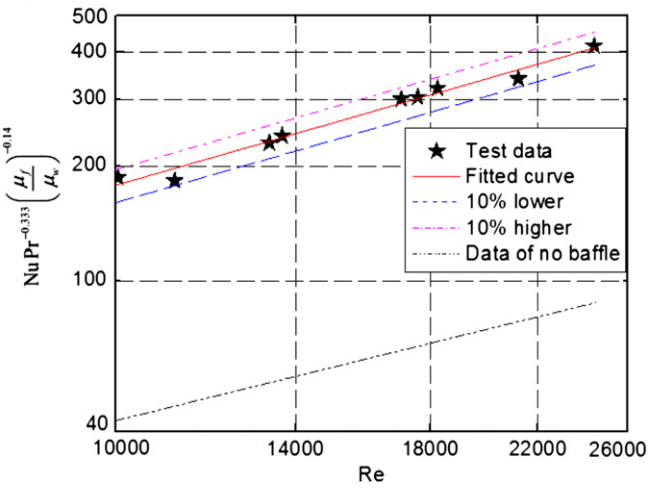

Fig. 4. Variation of the shell-side performance of heat transfer with the Reynolds number.

fluctuations of experimental data, both the curves of 10% lower and higher than fitted values are computed and presented in Figs. 4–6 together with their experimental data.

3. Numerical simulation

The above experimental investigation has demonstrated that the shell side of THB-STHX has a good heat transfer performance. To reveal the underlying mechanism, we take the case of $Re = 10{,}000$ as an example, and numerical simulation is performed for this case. As the computation load is too heavy to model the whole heat exchanger with the CFD method, instead, the section between two baffles of a unit channel (see Fig. 1(b)) is selected as the computation region. Periodical boundary is adopted, in which the fluid parameters at the inlet and outlet are coupled. The geometrical model and meshes are generated with the software Gambit 2.3, as shown in Fig. 7. Structural grids are adopted in the mesh generation, and hexahedral elements are generated for the whole computation domain. In addition, the refinement is carefully conducted near the walls for the consideration of $y+$ on walls.

Commercial software Fluent 6.3 of double-precision version acts as the solver, and the steady incompressible turbulent flow model

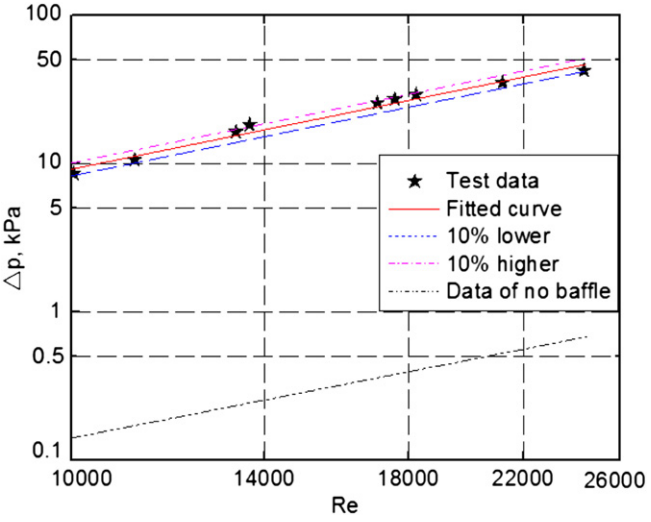

Fig. 5. Variation of the shell-side pressure loss with the Reynolds number.

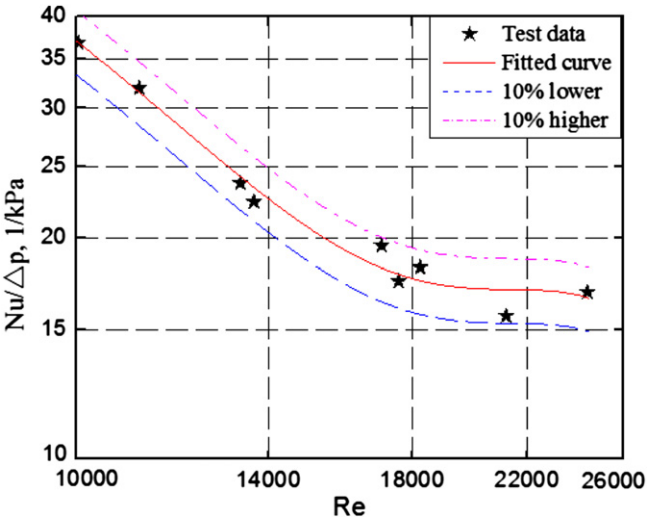

Fig. 6. Variation tendency of $Nu/\Delta p$ with the Reynolds number.

is adopted for the numerical computation. The conservation equations of continuity, momentum and energy in the Cartesian coordinate system are presented below in the tensor form.

Continuity equation:

$$\frac{\partial(\rho u_j)}{\partial x_j} = 0 \tag{14}$$

Momentum equation:

$$\frac{\partial(\rho u_i u_j)}{\partial x_j} = -\frac{\partial p}{\partial x_j} + \frac{\partial}{\partial x_j}\left(\mu_{\text{eff}}\left(\frac{\partial x_i}{\partial x_j} + \frac{\partial x_j}{\partial x_i}\right)\right) \tag{15}$$

Energy equation:

$$\frac{\partial(\rho c_p T u_j)}{\partial x_j} = u_j\frac{\partial p}{\partial x_j} + \frac{\partial}{\partial x_j}\left(\lambda_{\text{eff}}\left(\frac{\partial T}{\partial x_j}\right)\right) \tag{16}$$

where μ_{eff} is the effective dynamic viscosity, which is the sum of laminar and turbulent dynamic viscosity, i.e., $\mu_{\text{eff}} = \mu_l + \mu_t$, while λ_{eff} is the effective thermal conductivity.

Two-layer standard k–ε turbulence model with enhanced wall treatment is adopted for turbulent quantities [30]. The conservation

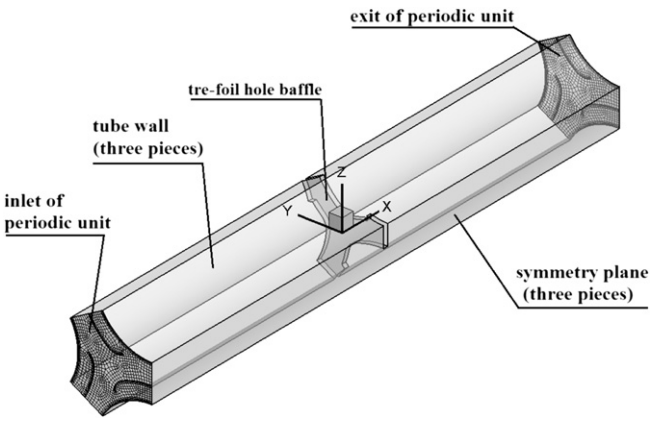

Fig. 7. Computation domain and meshes of the periodic model for a heat exchanger with trefoil-hole baffles, the scale between x axis and y or z axis is 0.5.

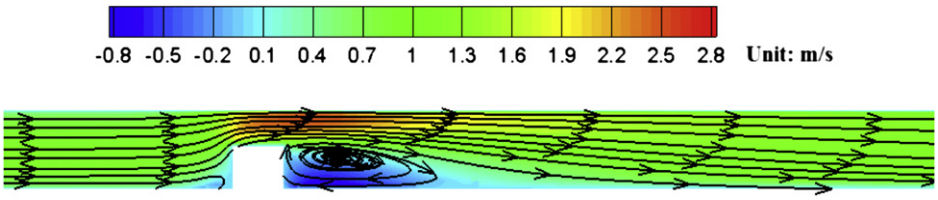

Fig. 8. Streamlines and axial-velocity contour near the baffle at the symmetry plane of unit channel for THB-STHX.

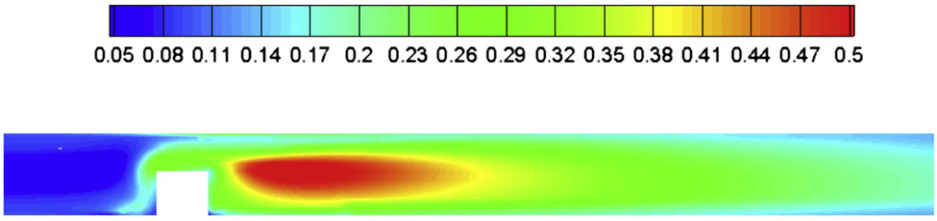

Fig. 9. Turbulence intensity contour near the baffle at the symmetry plane of unit channel for THB-STHX.

equations of turbulent kinetic energy (k) and turbulent kinetic energy dissipation rate (ε) are given below:

For turbulent kinetic energy k:

$$\frac{\partial(\rho k u_j)}{\partial x_j} = \frac{\partial}{\partial x_j}\left(\left(\mu_l + \frac{\mu_t}{\sigma_k}\right)\frac{\partial k}{\partial x_j}\right) + G_k - \rho\varepsilon \tag{17}$$

For turbulent kinetic energy dissipation rate ε:

$$\frac{\partial(\rho \varepsilon u_j)}{\partial x_j} = \frac{\partial}{\partial x_j}\left(\left(\mu_l + \frac{\mu_t}{\sigma_\varepsilon}\right)\frac{\partial \varepsilon}{\partial x_j}\right) + \frac{C_{1\varepsilon}\varepsilon}{k}G_k - C_{2\varepsilon}\rho\frac{\varepsilon^2}{k} \tag{18}$$

where $\mu_t = \rho C_\mu (k^2/\varepsilon)$,

$$G_k = 2\mu_t E_{ij}\cdot E_{ij}; \quad E_{ij} = (1/2)\left((\partial u_i/\partial x_j) + (\partial u_j/\partial x_i)\right)$$

.

The constants for the standard k–ε turbulent model are set as below:

$$C_\mu = 0.09;\ C_{1\varepsilon} = 1.44;\ C_{2\varepsilon} = 1.92;\ \sigma_k = 1.0;\ \sigma_\varepsilon = 1.3$$

The finite volume method is adopted for the discretization, and all the variables are treated with the second-order upwind scheme, except the pressure term with standard scheme. Numerical computations are conducted with the pressure-based solver, and pressure and velocity are coupled with the 'SIMPLE' algorithm. Enhanced wall treatment is adopted for the modeling of near-wall region. The convergent criterions are set as: relative residual of 1E−8 for energy and 1E−5 for other variables. The numerical model was validated through a simulation of the unit channel of STHX without baffles under the turbulent flow regime, and the Nusselt number and friction factor both match with the well-known correlations of Eqs. (6) and (11).

The shell-side convective heat transfer coefficient is calculated through Eq. (19), and the Nusselt number can then be obtained with Eq. (9).

$$h_s = \frac{Q_w}{S\cdot\left(T_{f,m} - T_{w,m}\right)} \tag{19}$$

Here, $T_{f,m}$ and $T_{w,m}$ are the averaged shell-side temperatures of the fluid and tube wall, respectively.

Grid independence of the results has been checked and about 2,000,000 cells are used in the final computation. The Reynolds number is 10,000, which corresponding to a flow rate of 0.068 kg/s in the unit channel. Constant temperature boundary condition is set upon the tube wall. The computation result shows that the average value of $y+$ on walls is about 2.4, and the convective heat transfer coefficient and pressure loss are ~8990 W/(m^2 K) and ~6.284 kPa/m, respectively, while the counterparts of the experimental results are ~9400 W/(m^2 K) and 6.57 kPa/m, respectively. The relative discrepancies of both convective heat transfer coefficient and pressure loss are within 5%, which demonstrates that the CFD simulation is of reasonable precision.

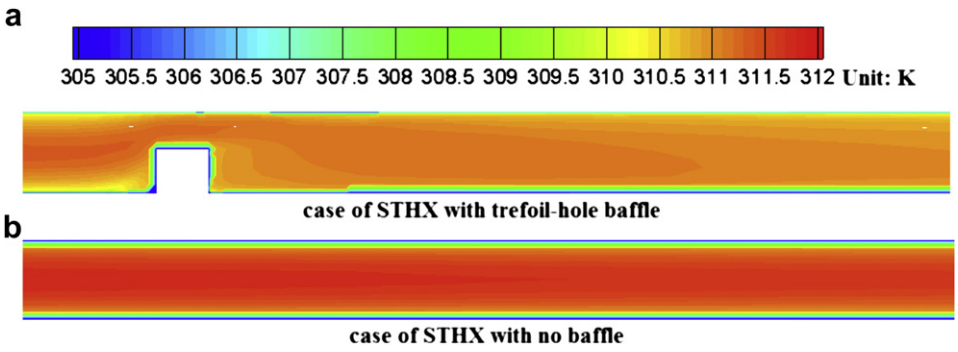

Fig. 10. Temperature contour near baffle at the symmetry plane of unit channel for THB-STHX and STHX without baffles.

To help analyzing the mechanisms of the thermo-hydraulic characteristics, we present the contours of velocity, turbulence intensity and temperature of the symmetry plane of the unit channel, as shown in Figs. 8–10.

Fig. 8 presents both the streamlines and axial-velocity contour near the baffle. It is clearly seen that the fluid velocity increases sharply at the breach of trefoil-hole baffle and washes against the downstream tube wall severely, which leads to a significant enhancement of the heat transfer rate. Moreover, a remarkable recirculation region is formed behind the baffle, while a weaker one emerges before the baffle due to its blockage to the jet flow. These reverse flows result in considerable pressure loss of the working fluid.

The variation of turbulence intensity near the baffle is shown in Fig. 9. It is clear that the turbulence intensity level increases substantially after the baffle, which implies that the flow resistance will be increased and the heat transfer rate will also be enhanced effectively.

The temperature contour of the symmetry plane of unit channel is depicted in Fig. 10(a) for THB-STHX, and the counterpart of STHX without baffles is presented in Fig. 10(b) for comparison. It is seen that due to the high-speed flush, high turbulence intensity level and strong reverse flow, most of the thermal boundary layer of THB-STHX is much thinner as compared with that without baffles. This implies that the near-wall temperature gradient is larger in the case with trefoil-hole baffles, therefore, heat transfer is effectively augmented on the shell side, as a result, the exit temperature of working fluid is much lower than the case without baffles, as clearly seen in Fig. 10.

4. Conclusions

Thermo-hydraulic performances on the shell side of a shell-and-tube heat exchanger with trefoil-hole baffles (THB-STHX) were experimentally investigated under the turbulent flow regime with the Reynolds number ranging from ~10,000 to 25,000 in the present study. Empirical correlations of the Nusselt number and pressure drop on the shell side have been obtained through data fitting. It is shown that the THB-STHX has a good performance of heat transfer. The value of $NuPr^{-0.333}(\mu_f/\mu_w)^{-0.14}$ increases with the increment of the Reynolds number and its average value is ~280, which is about 4.5 times that without baffles. The flow resistance also increases with the Reynolds number. The combined parameter, $Nu/\Delta p$, decreases with the increment of the Reynolds number at a decreasing rate, and its value lies in the range of 16–37 kPa^{-1}. Numerical simulation of the unit channel shows that the trefoil-hole baffle could generate the high-speed flush against downstream tube wall and intensive recirculation flow, as well as high turbulence intensity level. As a result, temperature boundary thickness near the wall is significantly reduced and the heat transfer rate is considerably enhanced, accompanied by a pronounced increase in the flow resistance. In addition to the good thermo-augmentation performance, THB-STHXs are easy to manufacture, and less liable to be fouled, which makes them promising to be widely applied in various industries.

Acknowledgements

This work was supported by the projects of Natural Science Foundation of China (No. 51076054, No. 51076057 and No. 51036003).

References

[1] S.W. Qian, Handbook for Heat Exchanger Design, Chemical Industry Press, Beijing, 2002 (in Chinese).
[2] A.E. Bergles, ExHFT for fourth generation heat transfer technology, Exp. Therm. Fluid Sci. 26 (2002) 335–344.
[3] A.W. Fan, J.J. Deng, J. Guo, W. Liu, A numerical study on thermo-hydraulic characteristics of turbulent flow in a circular tube fitted with conical strip inserts, Appl. Therm. Eng. 31 (2011) 2819–2828.
[4] J. Yang, M. Zeng, Q. Wang, A. Nakayama, Forced convection heat transfer enhancement by porous pin fins in rectangular channels, J. Heat Transfer – Trans. ASME 132 (2010) 051702-1–051702-8.
[5] J. Guo, A.W. Fan, X.Y. Zhang, W. Liu, A numerical study on heat transfer and friction factor characteristics of laminar flow in a circular tube fitted with center-cleared twisted tape, Int. J. Therm. Sci. 50 (2011) 1263–1270.
[6] A.W. Fan, J.J. Deng, A. Nakayama, W. Liu, Parametric study on turbulent heat transfer and flow characteristics in a circular tube fitted with louvered strip inserts, Int. J. Heat Mass Transfer 55 (2012) 5205–5213.
[7] Y.H. You, A.W. Fan, W. Liu, S.Y. Huang, Thermo-hydraulic characteristics of laminar flow in an enhanced tube with conical strip inserts, Int. J. Therm. Sci. 61 (2012) 28–37.
[8] W.M. Song, J.A. Meng, Z.X. Li, Optimization of flue gas turbulent heat transfer with condensation in a tube, Chin. Sci. Bull. 56 (2011) 1978–1984.
[9] K.J. Bell, Heat exchanger design for the process industries, J. Heat Transfer – Trans. ASME 126 (2004) 877–885.
[10] T. Tinker, Shell side characteristics of shell and tube heat exchangers, parts I, II, III, in: Proceedings of the General Discussion on Heat Transfer, Institution of Mechanical Engineers, London, 1951, pp. 89–116.
[11] J.W. Palen, J. Taborek, Solution of shell side flow pressure drop and heat transfer by stream analysis method, CEP Symp. Ser. (1969) 65–92.
[12] J.F. Guo, M.T. Xu, L. Cheng, The application of field synergy number in shell-and-tube heat exchanger optimization design, Appl. Energy 86 (2009) 2079–2087.
[13] H. Li, V. Kottke, Analysis of local shell side heat and mass transfer in the shell-and-tube heat exchanger with disc-and-doughnut baffles, Int. J. Heat Mass Transfer 42 (1999) 3509–3521.
[14] H. Li, V. Kottke, Effect of baffle spacing on pressure drop and local heat transfer in shell-and-tube heat exchangers for staggered tube arrangement, Int. J. Heat Mass Transfer 41 (1998) 1303–1311.
[15] H. Li, V. Kottke, Effect of the leakage on pressure drop and local heat transfer in shell-and-tube heat exchangers for staggered tube arrangement, Int. J. Heat Mass Transfer 41 (1998) 425–433.
[16] M. Prithiviraj, M.J. Andrews, Three-dimensional numerical simulation of shell-and-tube heat exchangers. Part II: heat transfer, Numer. Heat Transfer A – Appl. 33 (1998) 817–828.
[17] Y.L. He, W.Q. Tao, B. Deng, X. Li, Y. Wu, Numerical simulation and experimental study of flow and heat transfer characteristics of shell side fluid in shell-and-tube heat exchangers, in: Proceedings of Fifth International Conference on Enhanced, Compact and Ultra-Compact Heat Exchangers: Science, Engineering and Technology, Engineering Conferences International, Hoboken, NJ, USA, 2005, pp. 29–42.
[18] Q.W. Wang, G.N. Xie, M. Zeng, L.Q. Luo, Prediction of heat transfer rates for shell-and-tube heat exchangers by artificial neutral networks approach, J. Therm. Sci. 15 (2006) 257–262.
[19] R. Mukherjee, Effectively design shell-and-tube heat exchanger, Chem. Eng. Prog. (1998) 21–37.
[20] C.C. Gentry, Rod baffle heat exchanger technology, Chem. Eng. Prog. 86 (1990) 48–56.
[21] W. Liu, Z.C. Liu, Y.S. Wang, S.Y. Huang, Flow mechanism and heat transfer enhancement in longitudinal-flow tube bundle of shell-and-tube heat exchanger, Sci. China Ser. E – Technol. Sci. 52 (2009) 2952–2959 (in Chinese).
[22] X. Deng, S. Deng, Investigation of heat transfer enhancement of roughened tube bundles supported by ring or rod supports, Heat Transfer Eng. 19 (1998) 21–27.
[23] B. Peng, Q.W. Wang, C. Zhang, G.N. Xie, L.Q. Luo, Q.Y. Chen, M. Zeng, An experimental study of shell-and-tube heat exchangers with continuous helical baffles, J. Heat Transfer – Trans. ASME 129 (2007) 1425–1431.
[24] Y.G. Lei, Y.L. He, L. Rui, Y.F. Gao, Effects of baffle inclination angle on flow and heat transfer of a heat exchanger with helical baffles, Chem. Eng. Process. 47 (2008) 2336–2345.
[25] Y. Wang, Z. Liu, S. Huang, W. Liu, W. Li, Experimental investigation of shell-and-tube heat exchanger with a new type of baffles, Heat Mass Transfer 47 (2011) 833–839.
[26] S.J. Green, G. Hetsroni, PWR steam generators, Int. J. Multiphase Flow 21 (1995) 1–97.
[27] J.P. Holman, Heat Transfer, McGraw-Hill, New York, 1997.
[28] N. Sahiti, F. Krasniqi, Xh. Fejzullahu, J. Bunjaku, A. Muriqi, Entropy generation minimization of a double-pipe pin fin heat exchanger, Appl. Therm. Eng. 28 (2008) 2337–2344.
[29] A.J. Wheeler, A.R. Ganji, Introduction to Engineering, Prentice-Hall, Englewood Cliffs, 2004.
[30] Fluent V6.3 User Guide, Fluent Corporation, Lebanon, New Hampshire, 2006.